Spatial Channel Characterization for Smart Antenna Solutions in FDD Wireless Networks

Mark Beach, *Associate Member, IEEE*, Ben Allen, and Peter Karlsson

***Abstract*—This paper introduces a novel metric for determining the spatial decorrelation between the up- and down-link wireless bearers in frequency division duplex (FDD) networks. This metric has direct relevance to smart or adaptive antenna array base-station deployments in cellular networks, which are known to offer capacity enhancement when compared to fixed coverage solutions. In particular, the results presented were obtained from field trial measurement campaigns for both urban and rural scenarios, with the observations having a direct impact on the choice of down-link beamforming architecture in FDD applications. Further, it is shown that significant spatial decorrelation can occur in urban deployments for bearer separations as small as 5 MHz. Results are presented in terms of both instantaneous characteristics as well as time averaged estimates, thus facilitating the appraisal of smart antenna solutions in both packet and circuit switched networks.**

***Index Terms*—Adaptive arrays, frequency division duplex (FDD) spatial propagation, smart antennas.**

I. Introduction

MOBILE communications continues to place tremendous pressures on the limited radio spectrum that is particularly well suited to current user applications and future trends [1]. In order to address this growing demand for wireless information, significant advances in modulation and coding continue to be made, thus improving the spectrum efficiency of the information-bearing signal. Smart, or adaptive antennas offer a complementary solution to enhancing spectrum efficiency by exploiting the spatial, or both the spatial and temporal domains of the signalling space[2]. Numerous researchers have reported capacity enhancements of between 200% to 300% from both theoretical and field trial based evaluations [3], [4] thus demonstrating the benefits of this technology to network operators and equipment manufacturers alike.

In order to ensure both robust and optimum deployment of smart antenna systems, detailed knowledge of the spatial and temporal radio channel properties is required by system and network designers. This paper builds on existing spatial propagation performance metrics by considering a new measure, spatial correlation bandwidth, thus obtaining a greater insight to the frequency-spatial dependence of these systems. This new metric has particular relevance to smart antenna systems operating in conjunction with a frequency division duplex (FDD) air interface as developed and discussed here.

This paper is organized as follows. Section II introduces the concepts and architectures behind smart antenna systems for capacity enhancement, with Section III introducing spatial performance measures that can be employed to aid the bench marking of such systems. The measurement hardware design and customization which was central to the field trial, as well as the campaigns, are described in Sections IV and V, respectively. Data analysis applicable to FDD deployments is presented in Section VI alongside conclusions and observations in Section VII.

II. Smart Antennas for Capacity Enhancement

A smart antenna system employs a number of sensors to spatially sample the environment. In wireless systems the sensors are antenna elements, usually comprising of a number of linearly spaced devices that collectively form an array [5]. When these elements are closely spaced, with separations approaching 0.5 λ (where λ is the carrier wavelength), individual phase control can be applied to the output of each element prior to summation in order to spatially steer the radiation pattern or beam. Furthermore, amplitude weights can also be applied to control the profile of the main beam and side-lobe structure.

Cellular radio systems, such as the Universal Mobile Telecommunication System Terrestrial Radio Access (UMTS-UTRA) standard, are self-interference limited since users occupy the same carrier and time slot and are separated by using pseudo-random codes [6]. Spatial control of the beam pattern, or spatial filtering, offered by a smart antenna array deployed at a basestation can be used to reduce the amount of interference present [7], thereby facilitating the support of more simultaneous users within the network. This technique is known as spatial filtering for interference reduction (SFIR). Where appropriate, this technique can be extended to simultaneously multiplex time, frequency and code domains within the visible region of the array aperture to offer capacity enhancement by means of space division multiple access (SDMA), although this approach is deemed not to be required for UTRA deployments.

In a bi-directional communications link, such as UTRA, separate radio channels exist to convey the information "to" and "from" the mobile terminal with the basestation. These are usually referred to as the "downlink" and "uplink" channels respectively and can be allocated using either frequency division duplex (FDD) or time division duplex (TDD). In TDD applications it is possible to exploit the smart antenna uplink weights (phase and amplitude settings) on the downlink provided that the duplex frame period is within the coherence

Manuscript received July 25, 2002; revised February 20, 2003. This paper was supported by the UK EPSRC/HEFCE JREI'98 award supporting the procurement of the Medav RUSK measurement system.

M. Beach is with the University of Bristol, Bristol BS8 1TH, U.K. (e-mail: M.A.Beach@Bristol.ac.uk).

B. Allen is with the Centre for Telecommunications Research, Kings College, University of London, London WC2R 2LS, U.K. (e-mail: Ben.Allen@iee.org).

P. Karlsson is with Telia Research AB, SE-977 75 Lule, Sweden (e-mail: Peter.C.Karlsson@telia.se).

Digital Object Identifier 10.1109/TAP.2003.820948

time of the channel, i.e., the spatial-temporal characteristics of the channel remain constant during this period. Here, techniques such as temporal reference beamforming (TRB) [8] can be readily applied to both links, by exploiting embedded training sequences and computing the optimum weight vector. For wireless links with a round-trip delay in excess of "tolerable" latency, FDD is usually employed. This is often the case for outdoor mobile applications, however, FDD networks create additional challenges to the smart antenna system designer as outlined below.

A. Downlink Beamforming for FDD Applications

Optimum uplink weight vector calculation can be employed in FDD applications provided that suitable training sequences or symbols exist, as is the case for UTRA FDD. However, this uplink weight vector obtained by TRB processing can not be directly reapplied to the downlink, as the FDD frequency spacing is usually outside the coherence bandwidth of the channel, where the magnitude of the instantaneous fading is un-correlated between the up- and down-links. Here methods such as feedback or semi-blind beamforming can be employed in order to obtain suitable downlink weight vectors.

In the case of feedback downlink beamforming [9], a probing signal is used to optimize the weights, however this can significantly increase the signalling overheads in the network. In semi-blind downlink beamforming solutions, channel estimates are derived from the uplink [10], and this approach can be simplified to a switched beamformer utilising the same up- and down-link look directions [11]. This paper address the robustness of the semi-blind beamforming of the downlink based on the spatial response, or spatial reference beamforming (SRB) derived from the uplink.

III. Performance Metrics

Classical performance metrics such as BER and $\mathrm{E_b/N_0}$ have enabled system level performance of smart antennas to be ascertained [4], [12] by numerous researchers. Here, performance measures specifically tailored to assess the performance of semi-blind, or SRB downlink beamforming, based on frequency selective spatial channel characteristics are introduced.

A. Power Azimuth Spectrum (PAS)

The PAS is a frequently used measurement describing the spatial distribution of the signal sources illuminating an access point or base-station. The RMS azimuth spread (σ_θ), [13],[14] is often defined as the second central moment of the estimated PAS $(\hat{\mathrm{p}}(\theta))$, as given by (1) for a discrete PAS averaged over the impulse response data. Whereas, the power delay azimuth spectrum (PDAS) describes the azimuth distribution of energy as a function of signal delay[1]. The results presented here focus on the PAS, therefore decoupling the beamformer operation from the need to support wideband signal manipulation. This approach facilitates the integration of the smart antenna facet with existing cell-site equipment. Note however that the analysis presented here can be extended to consider the frequency dependent correlation of each time delay bin. For the results presented in Section VI, the PAS was computed using the unitary ESPRIT algorithm [15] with a 15 dB impulse response dynamic range threshold and 4° angular resolution. Note that the RMS azimuth spread can be considered as the azimuth domain equivalent to RMS delay spread [16] and is considered to be a robust computation of σ_θ for spreads of less than 45°[17], which is generally the case for the environments considered here

$$\sigma_\theta = \sqrt{\frac{\sum_{\mathrm{k}=1}^{\mathrm{K}} (\theta_\mathrm{k} - \psi_a)^2 \cdot \hat{\mathrm{p}}(\theta_\mathrm{k})}{\sum_{\mathrm{k}=1}^{\mathrm{K}} \hat{\mathrm{p}}(\theta_\mathrm{k})}}. \tag{1}$$

Where $\psi_a = \sum_{\mathrm{k}=1}^{\mathrm{K}} \theta_\mathrm{k} \cdot \hat{p}(\theta_\mathrm{k}) / \sum_{\mathrm{k}=1}^{\mathrm{K}} \hat{p}(\theta_\mathrm{k})$ and $\hat{\mathrm{p}}(\theta_\mathrm{k})$ is the power of the $\mathrm{k^{th}}$ ray arriving at angle θ_k.

B. Spatial Correlation Bandwidth

In order to appraise the frequency sensitive structure of the PAS, the term spatial correlation bandwidth is defined here [18]. Correlation, as defined in [19], facilitates the calculation of the frequency offset at which the PAS becomes decorrelated below a target threshold. This concept is analogous to the method used to compute correlation bandwidth [20] of a channel, however the principal difference being that the correlation coefficient of the PAS is computed instead of the channel frequency response. The spatial correlation bandwidth of the channel data obtained during the field trials described in Sections V and VI was computed using the following method:

a) The PDAS was computed using the 1-D unitary ESPRIT algorithm [15]. (For the results presented here, the impulse response data was windowed to a 15 dB dynamic range to have comparable conditions between peaks and weaker components at all measurement locations and exclude the unwanted effects of system noise. Further, a 5-MHz channel bandwidth was assumed and averaging over 16 channel snapshots was employed.)

b) The PDAS was time-delay averaged to remove wideband-fading artefacts to give the resultant PAS. (Here, the averaging length was equal to the probing signal period, 6.4 μs and 12.8 μs for the urban and rural environments respectively). This gives a measure of the total received power as a function of angle of arrival for each specific frequency of interest.

c) Computation was then repeated for multiple discrete frequency offsets (0 to 15 MHz in 156.25 kHz steps). From this data, the correlation coefficient (ρ_{ij}) was then computed between each PAS pair using (2)

$$\rho ij = \left| \frac{Rij}{\frac{1}{N}\sqrt{\left[\sum_{n=0}^{N-1} \hat{p}_i^2(\theta_n) \cdot \sum_{n=0}^{N-1} \hat{p}_j^2(\theta_n)\right]}} \right|. \tag{2}$$

Where $\mathrm{R_{ij}}$ is the cross correlation at zero lag of the PAS with $\hat{p}_i(\theta_n)$ and $\hat{p}_j(\theta_n)$ sampled at angle θ_n and N is the number of independent samples in $\hat{\mathrm{p}}(\theta_n)$ (here, $\mathrm{N} = 1$). An $\mathrm{I} \times \mathrm{J}$ correlation coefficient matrix containing the correlation coefficients for each PAS pair is then constructed.

[1]Also known as a Scatter map or 2-D-PAS.

By averaging over each of the matrix diagonals, the PAS correlation can be determined as a function of frequency offset. Section VI contains numerous examples of results obtained using this procedure.

IV. Measurement System Design

The wideband multisensor field trial data presented in Section V was obtained by means of customization and integration of a 1.9 GHz panel antenna array with a commercially available wideband vector signal analyzer. The hardware customization and array calibration required to complete the measurement system is now described in brief.

A. Wideband Vector Signal Analyzer

The measurement system employed a state-of-the-art wideband vector channel sounder (Medav RUSK BRI [21]) in order to obtain the complex frequency domain characteristics from a multielement receiving array. This hardware can be configured to operate at either 5.2 GHz or between 1.8 and 2.5 GHz (selectable in 100 MHz steps), with a maximum internal RF output power of $+27$ dBm. The portable transmitter continuously emits a periodic multitone signal with a maximum bandwidth of 120 MHz and a variable period of between 0.8 μs and 25.6 μs. This parameter was set in accordance with the maximum expected propagation delay. The receiver, which was deployed as a basestation, has an accurate copy of the transmitted waveform by means of "back-to-back calibration" and the physical parameters of the transmission medium under investigation are obtained by frequency domain manipulation of this waveform with the received signal. The transmitter and receiver have thermally stabilised rubidium clocks in order to assure temporal stability of the measured data.

Spatial-temporal channel characterization was conducted using this equipment within the frequency band 1910 to 1930 MHz, corresponding to the lower portion of the UTRA uplink spectrum allocation in the UK and within the operating bandwidth of the receiving array described below. Hence, the spatial correlation bandwidth of a wireless network operating at a carrier frequency of approximately 1.9 GHz with 5 MHz channelization within an operational spectrum of 20 MHz can be directly calculated using this equipment.

B. Multielement Receiving Array

The receiving array on loan from Allgon Systems AB [22] was fabricated from eight identical vertical columns deployed in a uniform linear array format with an element spacing[2] of 0.544 λ at 1920 MHz. Each column comprised of a fixed subarray of eight vertically stacked dual polarized ($\pm 45°$) elements providing 3 dB azimuth and elevation beamwidths of approximately 120° and 7.5° respectively. This equates to a column gain of approximately 17 dBi. Further, the array had no electrical down-tilt, thus additional mechanical down-tilt was applied during the trials.

A customized high-speed multiplexer and associated control circuitry provided the interface between the 16 output ports of the Allgon array to the Medav RUSK receiver input as well as additional amplification, channel preselection and IF filtering. Multiplexing took place in two stages: first, a bank of eight parallel 2:1 multiplexers provided polarization switching, followed by an 8:1 multiplexer to switch between the subarrays as illustrated in Fig. 1.

[2]This was applied over $\pm 60°$ of visible space, however grating lobes were occasionally observed [23]

C. Mobile Transmitting Station

The mobile transmitting equipment was housed in an estate car, with radiation by means of an omni directional 2 dBi rooftop mounted sleeve dipole antenna at a height of 1.45 m. Additional RF power amplification at the output of the Medav transmitting unit was included in order to provide sufficient operating range for the trials, thus compensating for both path loss and receiver noise figure. The maximum available transmit power was $+43$ dBm, with continuous RF power monitoring by means of an in-line directional coupler and RF power meter.

D. System Calibration

Prior to each field trial deployment the measurement system was calibrated to ensure that only the wireless channel characteristics were observed. "Back-to-back" calibration by means of physically connecting the transmitter and receiver together via a known wired attenuation ensured that frequency references and system clocks were coherently aligned thus allowing accurate amplitude, phase and time-of-flight estimates to be made. This procedure also corrected for power amplifier gain and phase perturbations as well as filter group delay characteristics within the hardware line-up. The antenna array and high-speed multiplexer were excluded from the "back-to-back" calibration as the response of these components was measured as part the array calibration procedure and was assumed to be constant throughout the two week period of the trials.

Spatial calibration of the array was necessary in order to apply accurate spatial signal estimation analysis such as that offered by unitary ESPRIT. This was performed by means of estimating the mutual coupling matrix of receiving array and multiplexing circuitry in an anechoic chamber over azimuth angles of $\pm 90°$ in 1° intervals. The procedure consisted of measuring the eight subarray azimuth radiation patterns (on each polarization) and then estimating the correction matrix by means of the least squares algorithm described in [24]. The algorithm operates by optimising the array nulling capability for a mean squared error as defined at the array output with a correction matrix estimate applied. The nulling approach provides a steeper response than the alternative method of directly maximizing the array output. This procedure allows a direction of arrival estimation accuracy of better than 1° to be obtained [25].

E. Data Logging

The receiver data logging software was configured such that eight channel impulse responses (CIRs) were consecutively recorded for the $+45°$ polarization immediately followed by eight recordings on the $-45°$ polarization. Here, eight CIR's measurements on the same polarization are called a "snapshot." This was repeated so that 16 snapshots where recorded for

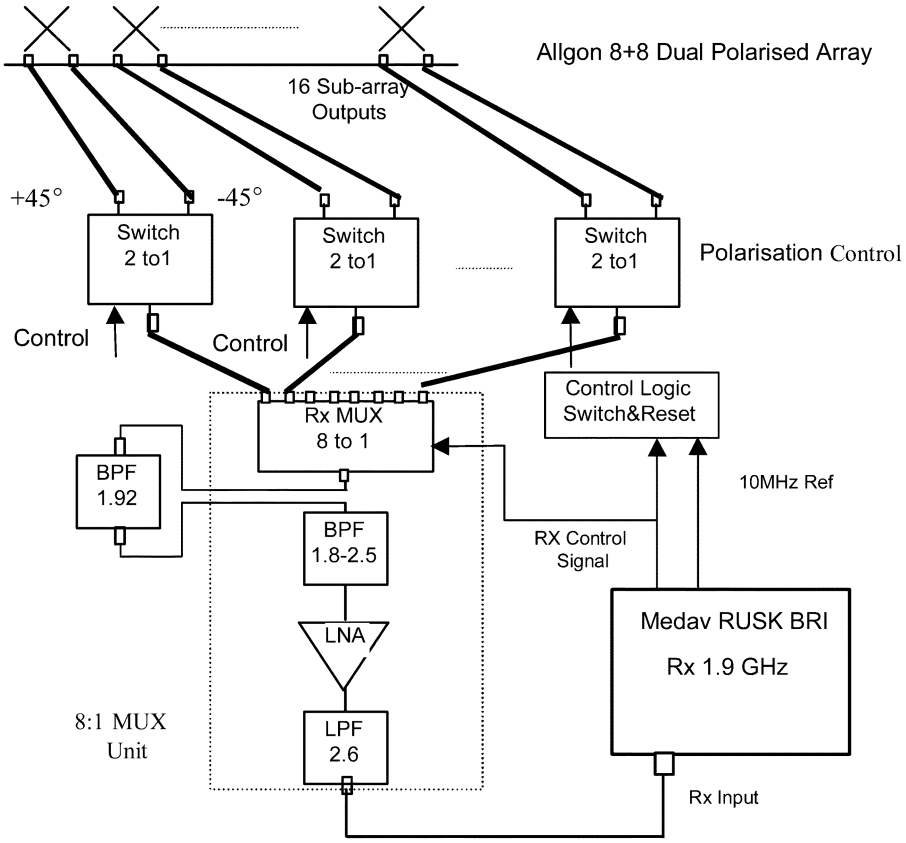

Fig. 1. Receiver architecture showing dual polar array multiplexer interface and associated circuitry.

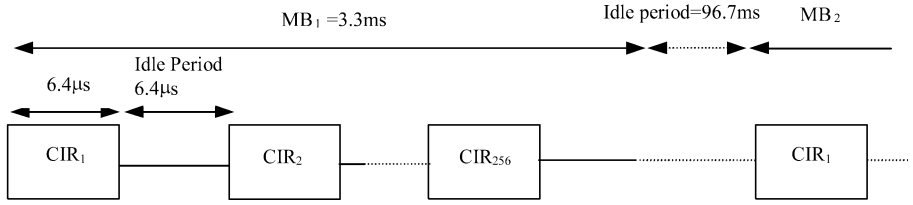

CIR_1= sub-array1, +45°, CIR_2= sub-array1, -45°… CIR_{32}= sub-array8, -45° etc.
1 snapshot= 8 CIR's, 1 MB= 32 snapshots

Fig. 2. Receiver timing and data structure.

each polarization (required for accurate direction of arrival estimation), giving 32 shapshots, termed here as a measurement block (MB). The associated received signal structure is shown in Fig. 2, where the total received signal period is assumed to be less than 6.4 μs (as was the case for the urban trials). The figure shows an idle period (6.4 μs in this case) which is required to allow the polarization switches and multiplexer to switch and settle before the next measurement was taken. The total measurement duration for each location was 10 s and during this period the MS remained on fixed location. Polarization deinterleaving of the data took place during postprocessing, which resulted in separate data files for each polarization. A unique feature of this system was that a complete snapshot was taken across the array within the coherence time of the channel under consideration, with the measurement period for one dual polar snapshot of all eight elements of 204.8 μs.

V. Field Trial Campaigns

An intensive field trial campaign was conducted over a two week period during July 2000 in the Bristol (U.K.) area using the customized channel sounding equipment described above. The measurement system was deployed in urban (small and large cell), indoor, outdoor-indoor, and rural (hilly and flat) scenarios [26], [27]. This paper focuses on the results obtain from both urban (small cell) and flat-rural deployments in terms of the spatial correlation bandwidth analysis for smart antenna applications in FDD networks, which were recorded during "busy-periods" of the day.

A. Urban Deployment

For the small cell urban deployment the measurement system was used to record the complex channel responses for all

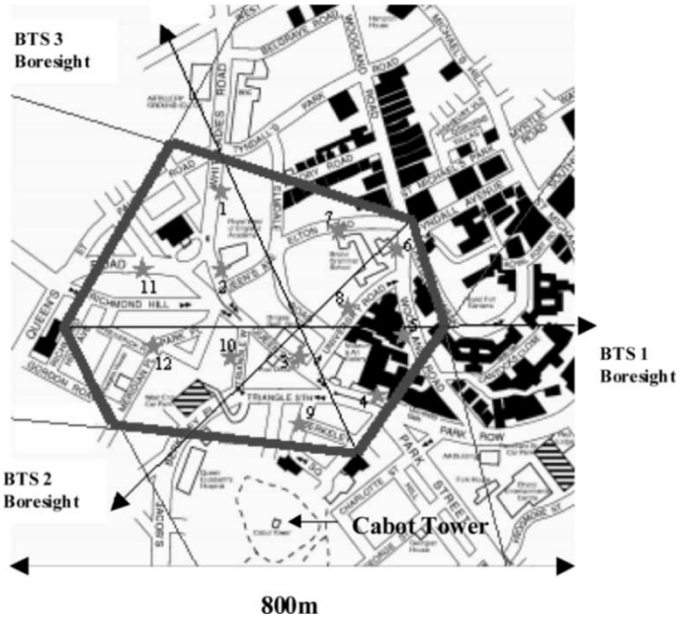

Fig. 3. Urban field trial location ($* = \mathrm{mobile}$ station).

combinations of three rooftop base-station (BTS) receiving locations and 12 mobile transmitting (MS) locations in the Clifton area of Bristol. Mechanical down-tilts of 5°, 7.5° and 5° were applied at the BTS locations respectively to ensure coverage of the area shown inside the thick line in Fig. 3, with Fig. 4 giving an indication of the local topography. The MS locations where uniformly distributed over the cell with ranges of between 50 and 650 m between the MS and BTS as shown on the map. Line-of-sight and non line-of-sight deployments were integrated into the trials plan, with examples of MS locations as given in Fig. 5. At each location 100 MBs were recorded in 10 s using a 6.4 μs probing signal period.

(a)

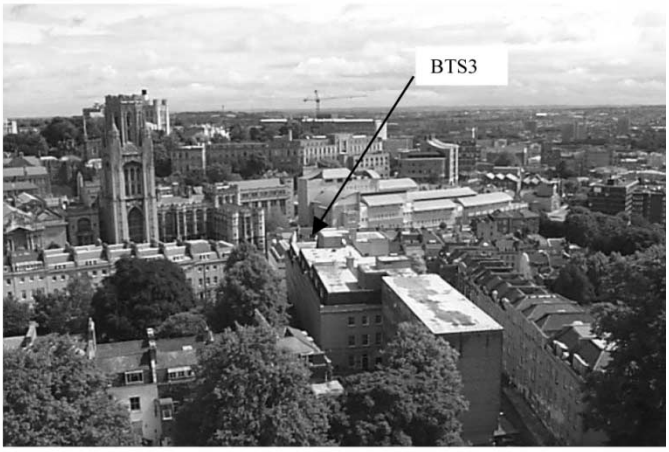

(b)

Fig. 4. (a) View from BTS3 (graduate school of education) and (b) view toward BTS3 from cabot tower (see Fig. 3).

B. Rural Deployment

Measurements were also taken within an uncluttered flat rural environment (border of Mendip Hills with the Somerset Levels, U.K.) for the purposes of performance comparisons. The scenario considered here is with the BTS located on Bleadon Hill, clear of any near-field scatterers and with a 6° down-tilt, as shown in Fig. 6. Channel measurements where taken from 13 MS locations situated around the level plain below the BTS site at ranges of between 1.2 and 4 km. The probing signal period was set to 12.8 μs for these trials due to the increased signal delay that results from the larger transmission ranges compared to the urban measurement environment described in the previous section. The MS distribution, array boresight and sector boundaries are shown in Fig. 7, with illustrations of the mobile locations as given in Fig. 8.

VI. Frequency Dependent Spatial Channel Analysis

The data collected during the field trial campaigns has been analyzed in terms of both temporal and spatial characteristics. Details describing the temporal analysis (delay spread, coherence bandwidth, and Rician K-factor) of the data can be found in reference [26] as well as the results from numerous system studies in [27] and [23]. These papers describe the application of dual polarized sensors in multiuser detection and performance degradation due to grating lobes when deploying antenna arrays in FDD networks. Also, an evaluation of "user location" by means of BTSs equipped with smart antennas is given in [28] based on the urban trial data presented here.

An analysis of the spatial channel decorrelation as a function of carrier frequency using both the PAS and spatial correlation bandwidth measures introduced in Section III for both measurement environments is now given. Results are presented for both instantaneous and time averaged measurements, with further details available in [29].

A. Small Urban Cell

The instantaneous DPAS for BTS1 operating with MS1 (see map in Fig. 3) is shown in Fig. 9, assuming 5 MHz channelization. Given that the hardware measurement system described in Section IV has a limited operational bandwidth, it is assumed here that the "uplink" utilizes the spectrum from 1910 to 1915 MHz and the "downlink" 1925 to 1930 MHz in order to ascertain any frequency dependent behavior of these channel. Note that this yields a 15 MHz frequency-offset between the

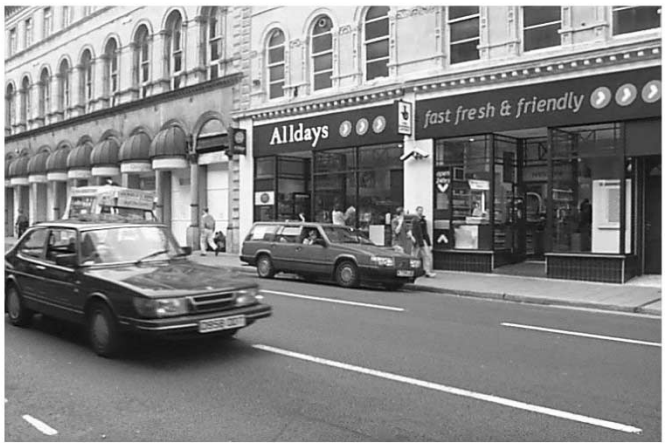

(a)

(b)

Fig. 5. (a) and (b) Example mobile locations taken during the urban trials.

Fig. 6. Rural BTS deployment on Bleadon Hill (U.K.).

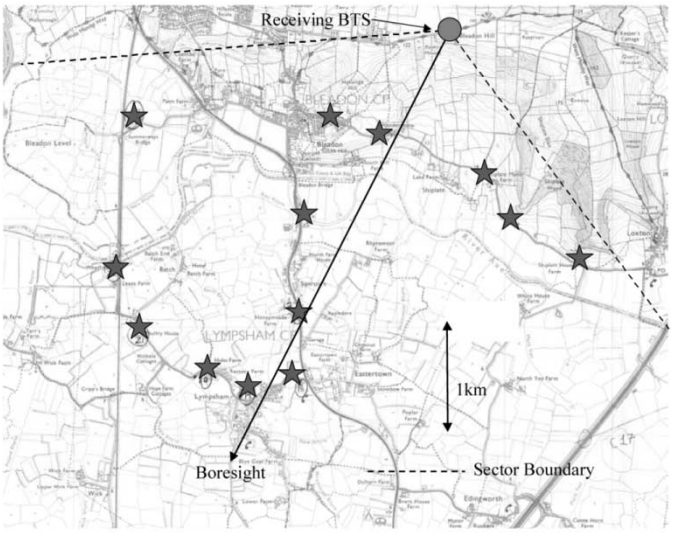

Fig. 7. Rural field trial scenario ($* = \mathrm{mobile}$ station) (Reproduced from Ordnance Survey maps by permission of Ordnance Survey on behalf of The Controller of Her Majesty's Stationary Office © Crown Copyright ED 100018292.).

sub-band centers. It can be clearly seen from this illustration that the spatial signatures of the "uplink" and "downlink" DPAS's are different. Fig. 10 gives the instantaneous PAS for the same location by averaging over the time delay bins. Clearly, the peak gain response iw displaced by some 5° in azimuth. This frequency sensitive behavior is further illustrated in Fig. 11 where the PAS is shown as a function of incremental frequency offset by sweeping the center frequency of the 5 MHz channel from 1912.5 to 1927.5 MHz in 156.25 kHz steps and computing the PAS at each increment. Here, a significant change in the PAS is observed for frequency offsets for as little as 4 MHz, when compared to the FDD channel spacing of UTRA [30].

The frequency sensitive behavior shown in Figs. 10 and 11 can be explained by considering the structure of the impulse response data contained within each snap-shot, since each individual PAS is computed for each 5 MHz sub-band as the measurement window is incremented over the entire 20 MHz band. As the sub-band is incremented, a different impulse response structure will occur as electrical dimensions of the channel change with frequency. For example, a typical street width of 30 m will vary from 214 λ wide on the downlink frequency to 195 λ on the uplink frequency for the UTRA FDD air interface [30] with a duplex spacing of 190 MHz. Therefore, the impulse response will change between the two bands accordingly, in particular that of the phase structure.

Spatial correlation bandwidth, as defined in Section III-B, can also be utilized in order to provide further characterization of the frequency sensitive behavior of the channel. The method described in Section III-B was applied to the urban data for BTS1 and MS8 and gives the frequency correlation function as displayed in Fig. 12. By selecting a correlation coefficient threshold (ρ_{th}), the spatial correlation bandwidth (B_θ) can be determined. The correlation function given in Fig. 12 yields $\mathrm{B}_\theta = 5.5\ \mathrm{MHz}$ for $\rho_{\mathrm{th}} = 0.5$ and $B_\theta = 928\ \mathrm{kHz}$ for $\rho_{\mathrm{th}} = 0.9$ respectively. For comparison purposes, the coherence bandwidth [26] of this location has a median value of 1.4 MHz. The choice of ρ_{th} is selectable by the system designer and will depend upon the amount of spatial decorrelation a downlink beamformer is likely to tolerate in order to maintain stable and

(a)

(b)

Fig. 8. (a) and (b): Examples of mobile station locations during rural trials.

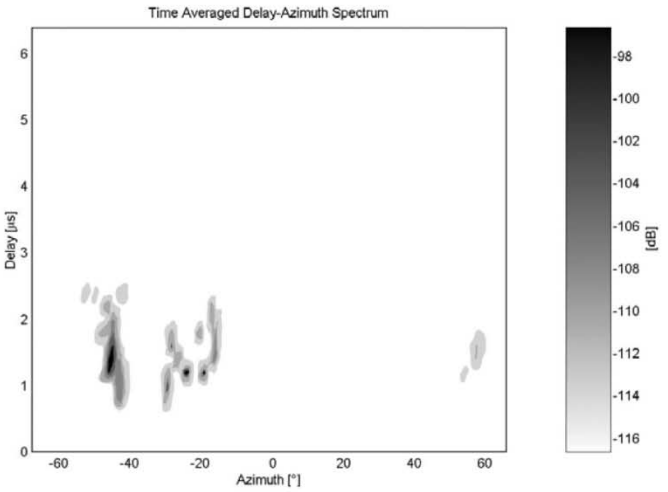

(a)

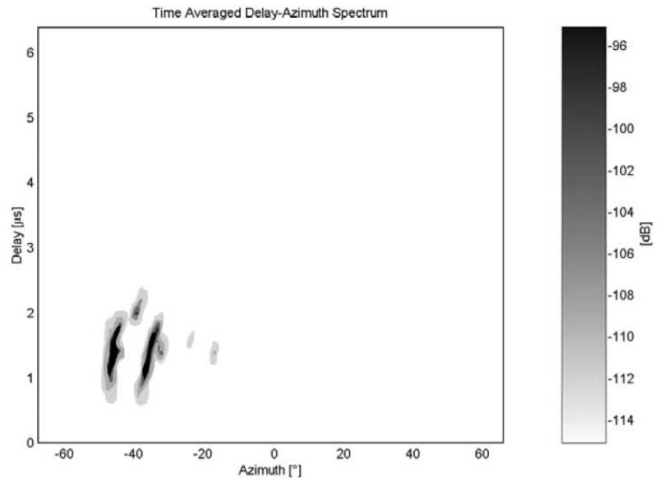

(b)

Fig. 9. PDAS for urban location BTS1 with MS1: (a) Uplink and (b) downlink.

robust operation. A high value of $\rho_{\rm th}$ is suitable for analysis of a system likely to have a low tolerance and a lower value is suited to systems likely to tolerate a higher degree of spatial decorrelation.

B. Flat Rural

An example of the instantaneous frequency sensitive behavior of the rural field trial data is given in Fig. 13 for one of the locations given within the map shown in Fig. 7 in order to facilitate a comparison between propagation environments. This figure was calculated using an identical procedure to that described in Section VI-A in order to produce Fig. 11 for the urban case. In contrast to the urban scenario, very little perturbation of the PAS is observed over the 20 MHz of spectrum under investigation, with a single stable spatial bearing of the transmitted signal being evident. Given that this rural deployment offers mainly a line of sight path to the mobile with an average Rician K-factor of 12 dB compared with -3 dB for urban scenario described previously, the impact of the frequency sensitive behavior of multipath will be significantly reduced. This result also validates the correct operation of the equipment, experimental procedures and post processing analysis of the data.

The spatial correlation bandwidth was calculated for this rural case yielding $\mathrm{B}_\theta = 13.8$ MHz for $\rho_{\rm th} = 0.5$ and $\mathrm{B}_\theta = 1$ MHz for $\rho_{\rm th} = 0.9$ respectively. However, for $\rho_{\rm th} = 0.5$, a number of results lie beyond the 15 MHz measurement window. Again for comparison purposes, the median value of the frequency coherence bandwidth of this environment [26] is 7.8 MHz. These results also demonstrate the frequency stability of the spatial response observed during the rural trials when compared with the urban case.

C. Temporal Averaging and Spatial Correlation Bandwidth

The spatial correlation bandwidths computed so far have been based on the instantaneous PAS. This is in direct contrast to the results reported by Pedersen *et al.* in [31], where the mobile station moved a distance of 40 λ during the measurement period of approximately 840 ms, thereby inherently applying both spatial and temporal averaging. In addition, the mobile operated at

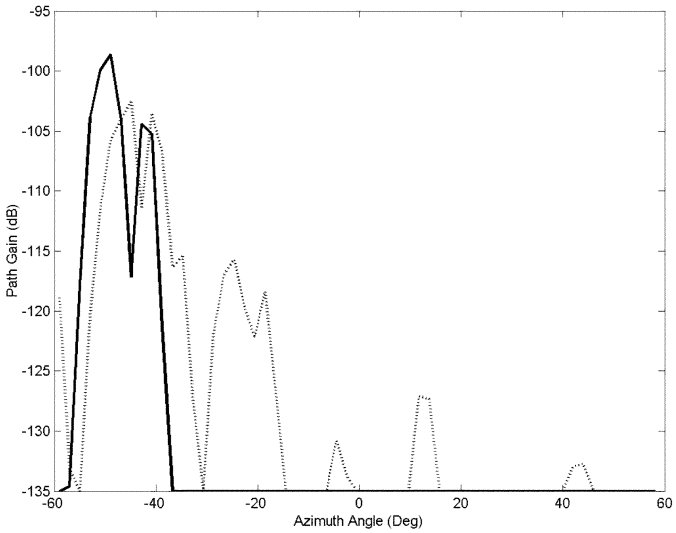

Fig. 10. Instantaneous PAS for urban BTS1 with MS1. Solid line: uplink and dotted line: downlink.

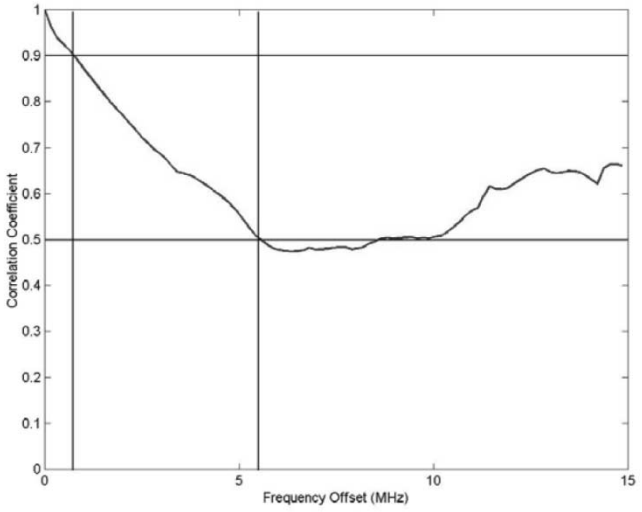

Fig. 12. Spatial correlation bandwidth.

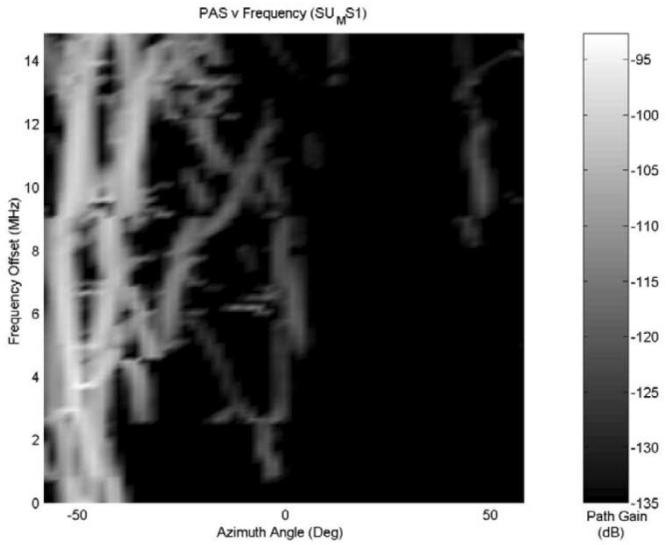

Fig. 11. Instantaneous PAS as a function of incremental frequency offset (urban BTS 1 with MS1).

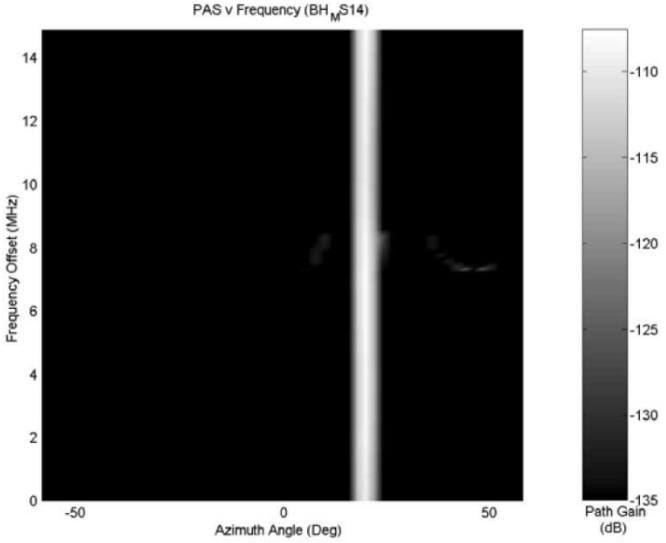

Fig. 13. Instantaneous PAS as a function of incremental frequency offset (rural environment).

a greater range than for the trials described here. The increased range yields a lower RMS azimuth spread, since the perceived scattering radius is smaller [14], having the effect of reducing the angular spread of energy. Although the nature of the field trials reported here have precluded spatial averaging from being applied due to the static MS, variable length temporal averaging is possible as the data is continuously logged over the 10 s measurement time window (see Fig. 2). The spatial correlation bandwidth is now computed from the urban trial data using PAS's averaged over 200 ms, 1 s, and 10 s, respectively.

Histograms for each averaging length are shown in Fig. 14(a)–(c) respectively, where B_θ has been computed for each of the urban deployments and appropriate temporal averaging applied. The spatial correlation results are summarized in Table I in terms of both average value and the maximum value observed ("mode"). It is clearly shown that, by applying temporal averaging of greater than the channel coherence time, the spatial correlation bandwidth is increased. In the histograms, spatial correlation bandwidth values of more than 15 MHz have been set to the maximum value (of 15 MHz) that can be recorded by the hardware. The results show that over 50% of observations where $\rho_{\mathrm{th}} = 0.5$ is used, the spatial correlation bandwidth is greater than 15 MHz, with this value increasing as the averaging time is increased. Note that the longer averaging periods to a lower absolute number of cases. Using the $\rho_{\mathrm{th}} = 0.9$ threshold highlights the differences between temporal averaging lengths over the 15 MHz of measurement available bandwidth. The $\rho_{\mathrm{th}} = 0.5$ results compare favorably with [31], where no significant differences were observed between the uplink and downlink PAS over the stated averaging parameters.

Full 10 s time averaging was applied to the data corresponding to BTS1 and MS1. The resulting temporally averaged PAS as a function of frequency offset from the lowest 5 MHz channel to the highest channel allocation within the band 1910

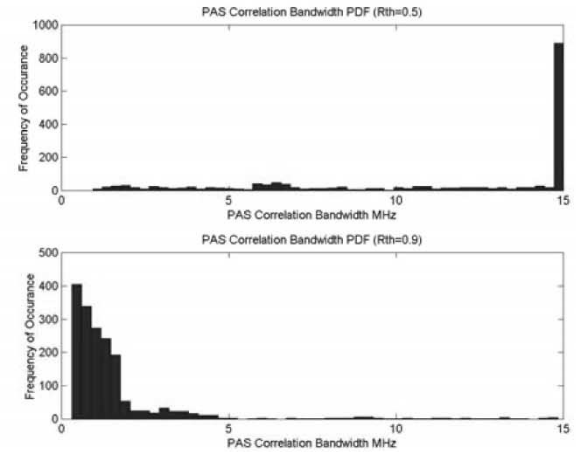

(a)

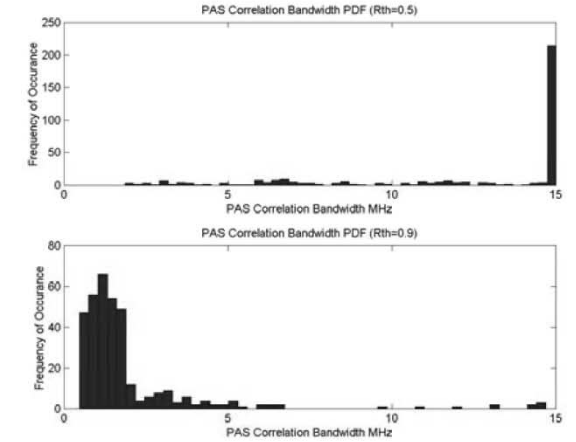

(b)

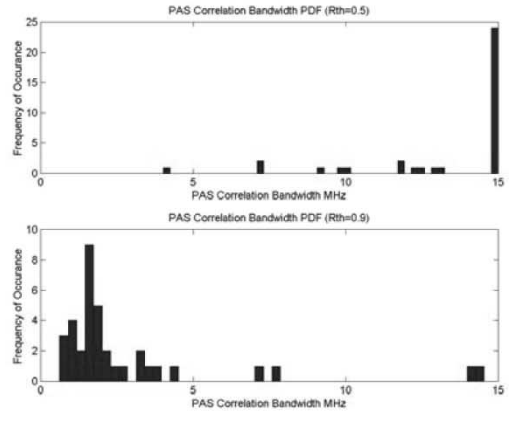

(c)

Fig. 14. Histograms of PAS correlation bandwidth for various temporal averaging lengths(a) 200 ms, (b) 1 s, and (c) 10 s.

to 1930 MHz. This is shown in Fig. 15 and when compared with Fig. 11 indicates that the underlying characteristics present in the incremental PAS are still present. Again, significant variation in the direction of arrival of dominant spatial components can be observed as well as the frequency sensitive creation of

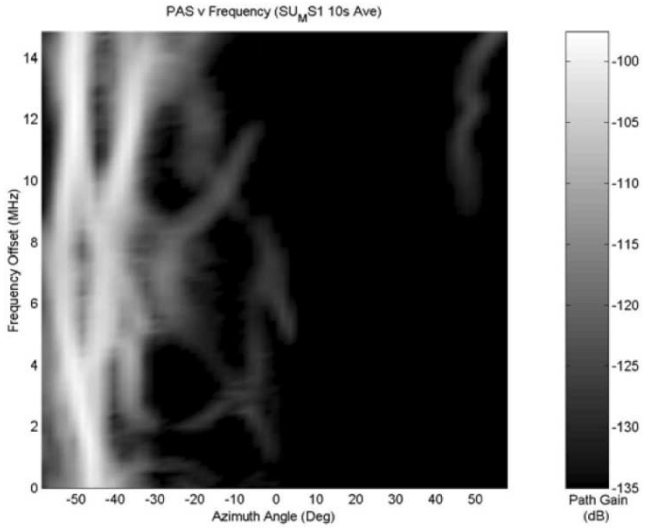

Fig. 15. Time averaged (10 s) PAS as a function of incremental frequency offset.

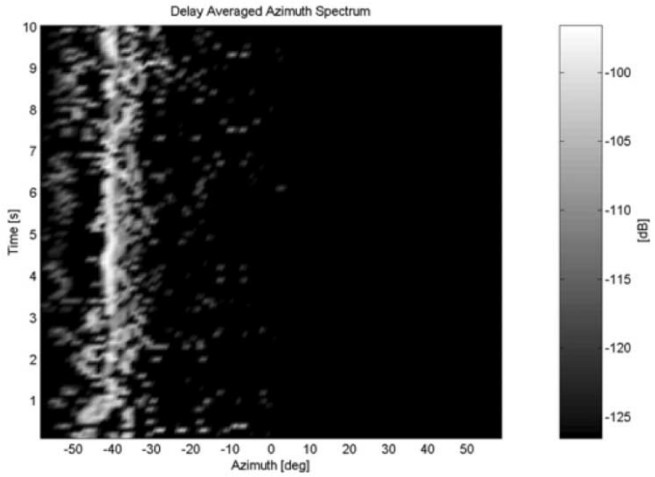

Fig. 16. Observed PAS as a function of time.

multiple spatial channels. A further indication of the dynamic behavior of this urban channel can be observed by examining the time history of the PAS obtained for the lowest 5 MHz channel over the full measurement window as given in Fig. 16. Here, the temporal fading of the channel can be seen over the full 10 s measurement period and as a function of azimuth angle. These results are contrary to those reported in [31] as discussed above.

VII. Discussion of Results and Conclusions

The results presented in Section VI indicate that the PAS displays a frequency sensitive behavior for the small urban cell trial data. In contrast, the spatial-frequency spectrum obtained from the flat rural environment illustrates very little change over the entire measurement band. This comparison serves as a validation of the measurement system and post processing tools that have been employed. The frequency sensitive behavior indicates the potential of suboptimum performance when uplink weights are applied directly to the downlink in FDD systems operating in cluttered environments.

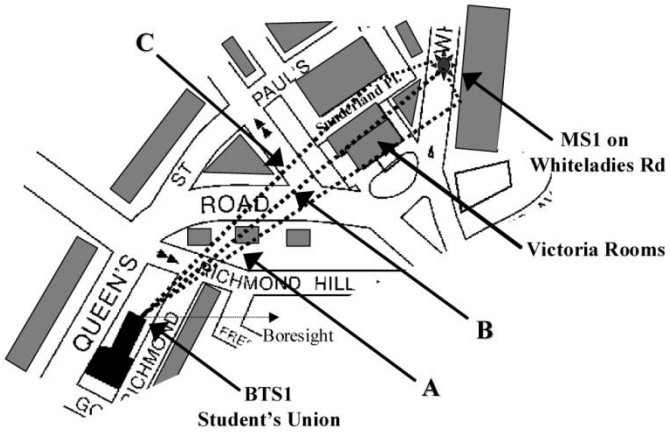

Fig. 17. Identification of frequency sensitive propagation paths.

TABLE I
SUMMARY OF SPATIAL CORRELATION BANDWIDTH STATISTICS FOR VARIOUS TEMPORAL AVERAGING LENGTHS (A) $\rho_{\text{th}} = 0.9$ (B) $\rho_{\text{th}} = 0.5$

AVERAGING TIME	200ms	1s	10s
Median (MHz)	0.6	0.85	0.85
Mode (MHz)	0.3	0.7	0.7

(a)

AVERAGING TIME	200ms	1s	10s
Median (MHz)	11.2	15	15
Mode (MHz)	15	15	15

(b)

A physical explanation of the results given in Figs. 11 and 15 can be obtained by considering the frequency sensitive summation of the multipath rays connecting MS1 with BTS1. The physical bearing of the mobile is $-42°$ from the Student's Union, with signal propagation by means of diffraction from side to front face of the Victoria Rooms at $-35°$ and ducting via Sunderland Place at $-52.5°$. These are labeled A, B, and C, respectively, in Fig. 17, with "A" providing the principal path by means of roof top diffraction over the Victoria Rooms at 0 MHz frequency offset, then both paths "B" and "C" providing the dominant mechanism at 7 and 15 MHz frequency offsets due to the frequency sensitive summation of the multipath components within the scattering volume adjacent to the mobile. Street ducting and roof-top diffraction have also been noted by other researchers [32] examining spatial propagation mechanisms within cluttered urban deployments.

The application of downlink beamforming without feedback in small cell cluttered urban environments is likely to be suboptimum for duplex spacings of greater than the spatial correlation bandwidth. The actual downlink directions of departure will differ from those estimated from the uplink, unless sufficient temporal averaging can be applied. This has an impact on packet based services, where transmission time can be within the same order of magnitude or even less than the channel coherence time, thereby precluding the application of temporal averaging. Conversely, connection oriented services, or services demanding frequent packet transmissions on the uplink readily allow the application of temporal averaging of the channel parameters, therefore reducing the impact of noise and temporal fading and considerably increasing the spatial correlation bandwidth as illustrated in Section VI-C. Although the choice of ρ_{th} is selectable by the system designer, it will depend upon the amount of spatial decorrelation that a downlink beamformer can tolerate in order to maintain stable and robust operation.

This work has identified a need for further propagation studies using equipment similar to that described here, but capable of working with the appropriate UMTS FDD spacings [33]. In addition, appraisal of the sensitivity of candidate beamforming architectures to the parameter ρ_{th} will provide a useful insight into the robustness and optimization of the candidate architectures. Further, a useful extension to the work presented here is to consider the frequency correlation of the PDAS that will aid the performance appraisal of wideband signal processing schemes such as 2-D spatial-temporal rake receivers.

ACKNOWLEDGMENT

The authors thank Allgon Systems AB for the generous loan of the antenna array. In addition, they thank D. McNamara, T. Vernon, J. Webber and other members of the CCR for their support during the field trials, Professors E. Bonek, R. Thomä and A. Nix for their useful comments on the work presented here, as well as the additional input from the reviewers of this paper.

REFERENCES

[1] "The Future Mobile Market: Global Trends and Developments With a Focus on Western Europe,", UMTS Forum Report, 1999.
[2] G. Tsoulos, J. McGeehan, and M. Beach, "Wireless personal communications for the 21st century: European technologies advances in adaptive antennas," *IEEE Commun. Mag.*, pp. 102–109, Sept. 1997.
[3] A. Naguib, A. Paulraj, and T. Kailath, "Capacity improvement with base-station antenna arrays in cellular CDMA," *IEEE Trans. Veh. Technol.*, vol. 43, pp. 691–698, Aug. 1994.
[4] M. A. Beach, C. M. Simmonds, P. Howard, and P. Darwood, "European smart antenna test-bed – Field trial results," *IEICE Trans. Commun.*, vol. E84-B, no. 9, pp. 2348–2356, Sept. 2001.
[5] R. C. Hansen, *Phased Array Antennas*. New York: Wiley, 1998.
[6] S. Dehghan, D. Lister, R. Owen, and P. Jones, "W-CDMA capacity and planning issues," *IEE Electron. Commun. J.*, vol. 12, no. 3, pp. 101–118, June 2000.
[7] J. Litva and T. Lo, *Digital Beamforming in Wireless Communications*. Norwood, MA: Artech House, 1996.
[8] L. Godara, "Application of antenna arrays to mobile communications, Part II: Beamforming and direction of arrival considerations," *Proc. IEEE*, vol. 85, no. 8, pp. 1195–1245, Aug. 1997.
[9] D. Gerlach and A. Paulraj, "Adaptive transmitting antenna arrays with feedback," *IEEE Signal Processing Lett.*, vol. 1, pp. 150–152, Oct. 1994.
[10] P. Zetterberg and B. Ottersten, "The spectrum efficiency of a base station antenna array system for spatially selective transmission," *IEEE Trans. Veh. Technol.*, vol. 44, pp. 651–660, Aug. 1995.
[11] C. Ward, D. Adams, F. Wilson, and A. Bush, "The live-air trial of a multi-beam cellular base station antenna system," in *Proc. Inst. Elect. Eng. Nat. Conf. Antennas and Propagation*, 1999, pp. 169–172.
[12] S. Tanaka, M. Sawahashi, and F. Adachi, "Pilot symbol-assisted decision-directed coherent adaptive array diversity for DS-CDMA mobile radio reverse link," *IEICE Trans. Fundamentals*, vol. E80-A, no. 12, pp. 2445–2452, December 1997.
[13] K. Pedersen, P. Mogensen, and B. Fleury, "A stochastic model of the temporal and azimuthal dispersion seen at the base station in outdoor propagation environments," *IEEE Trans. Veh. Technol.*, vol. 49, pp. 437–447, Mar. 2000.

[14] P. Eggers, "Angular dispersive mobile radio environments sensed by highly directive base station antennas," in *IEEE Vehicular Technology Conf. Proc.*, Toronto, Canada, 1995, pp. 522–526.
[15] M. Haardt and J. A. Nossek, "Unitary ESPRIT: How to obtain increased estimation accuracy with reduced computational burden," *IEEE Trans. Signal Processing*, vol. 43, pp. 1232–1242, May 1995.
[16] P. A. Bello, "Characterization of randomly time-variant linear channels," *IEEE Trans. Commun. Syst.*, vol. 11, pp. 360–393, Dec. 1963.
[17] P. Eggers, "Comparison of angular dispersion metrics in synthetic and measured radio channels," presented at the AP2000 Conf. Proc., Davos, Switzerland, Apr. 2000.
[18] M. Beach, B. Allen, and P. Karlsson, "Spatial decorrelation of frequency division duplex links," *IEE Electron. Lett.*, vol. 36, no. 22, pp. 1884–1885, Oct. 2000.
[19] E. Ifeachor and B. Jervis, *Digital Signal Processing: A Practical Approach*. Reading, PA: Addison-Wesley, 1996, pp. 183–213.
[20] M. P. M. Hall, L. W. Barclay, and M. T. Hewitt, "Propagation of radiowaves," *Inst. Elect. Eng.*, 1996.
[21] R. Thomä, D. Hampicke, A. Richter, G. Sommerkorn, A. Schneider, U. Trautwein, and W. Wirnitzer, "Identification of time-variant directional mobile radio channels," *IEEE Trans. Instrum. Meas.*, vol. 49, pp. 357–364, Apr. 2000.
[22] B. Lindmark, M. Ahlberg, M. Nilson, and C. Beckman, "Performance analysis of applying uplink estimates in the downlink beamforming using a dual polarized array," in *IEEE Vehicular Technology Conf. Proc.*, Tokyo, Japan, 2000.
[23] M. Hunukumbure, M. Beach, B. Allen, P. Fletcher, and P. Karlsson, "Smart antenna performance degradation due to grating lobes in FDD systems," presented at the COST260, Gothenberg, Sweden, May 2001.
[24] G. Sommerkamp, D. Hampicke, R. Klukas, A. Richter, A. Schneider, and R. Thomä, "Reduction of DOA estimation errors caused by antenna array imperfections," in *Proc. 29th Eur. Microwave Conf.*, Munich, Oct. 5–7, 1999, pp. 282–290.
[25] M. Beach, D. McNamara, and P. Karlsson, "Development of a channel measurement system for multiple-input multiple -Output (MIMO) applications," in *Proc. IST Mobile Communications Summit*, Galway, Eire, 1-4, 2000, pp. 497–501.
[26] B. Allen, J. Webber, P. Karlsson, and M. Beach, "'UMTS spatio-temporal propagation trial results'," in *Inst. Elect. Eng. ICAP2001 Conf. Proc.*, vol. 2, Manchester, U.K., Apr. 17-20, 2001, pp. 497–501.
[27] J. Webber, B. Allen, M. Beach, P. Karlsson, and N. Canagarajah, "Performance investigation of multiuser detectors employing a dual polarized antenna," in Proc. Eur. Personal and Mobile Communications Conf. (EMPCC), Vienna, Austria, Feb. 19-22, 2001.
[28] D. Kothris, M. Beach, B. Allen, and P. Karlsson, "'Performance assessment of terrestrial and satellite based position location systems," in *Inst. Elect. Eng. 3G2001 Conf.*, vol. 477, U.K., Mar. 26-28, 2001, pp. 211–215.
[29] B. Allen, "Smart Antennas for High Data Rate FDD Wireless Links," Ph.D. dissertation, Univ. Bristol, Bristol, U.K., 2001.
[30] "UTRA (BS) FDD; Radio Transmission and Reception," 3G Partnership Project, Doc. TS25.104 v3.0.0, 1999.
[31] K. Pedersen, P. Mogensen, and F. Frederiksen, "Joint directional properties of uplink and downlink channel in mobile communications," *IEE Electron. Lett.*, vol. 35, no. 16, pp. 1311–1312, Aug. 1999.
[32] A. Kuchar, J. P. Rossi, and E. Bonek, "Directional macro-cell characterization from urban measurements," *IEEE Trans. Antennas Propagat.*, vol. 48, pp. 137–146, Feb. 2000.
[33] S. E. Foo and M. A. Beach, "Uplink based downlink beamforming in UTRA FDD," presented at the COST 273 TD(02)104, Lisbon, Portugal, 2002.

Mark Beach (A'90) received the Ph.D. degree from the University of Bristol, Bristol, U.K., in 1989.

In 1989, he joined the University of Bristol as a member of academic staff where he currently holds the post of Professor of Radio Systems Engineering. He has made contributions to the European collaborative projects, TSUNAMI, SATURN, ROMANTIK, TRUST, and more recently SCOUT. At present his interests are focused toward multiple-input multiple-output (MIMO) channel characterization and the design and optimization of space-time coded wireless architectures for 3G and 4G wireless networks. His research interests include smart antenna technology for wireless as well as analogue RF circuitry for software definable radio (SDR).

Dr. Beach is an active Member of the Institution of Electrical Engineers (IEE) Professional Network on Antennas and Propagation as well as an Editor of the IEEE TRANSACTIONS ON WIRELESS COMMUNICATIONS.

Ben Allen received the M.Sc. and Ph.D. degrees from the University of Bristol, Bristol, U.K., in 1997 and 2001, respectively.

His postgraduate research included analyzing the application of smart antenna technology to high data rate wireless networks. This consisted of equipment customization, propagation trials and data analysis, as well as fundamental system performance analysis. Previously, he was a Research Assistant at Bristol University where he conducted research relating to outdoor and indoor propagation, spatial signal processing, antenna arrays, and wireless systems design. In 2001, he joined Tait Electronics Ltd., Christchurch, New Zealand, where he conducted post-doctorial research in the area of MIMO and space-time coding. He then joined the Centre for Telecommunications Research, King's College, University of London, London, U.K., as a Research Fellow, where he investigated the application of space-time codes to 4G wireless systems, and where he currently holds the post of Lecturer and assisted in establishing the Ultra Wideband Research Group.

Dr. Allen is a Member of the Institution of Electrical Engineers (IEE).

Peter Karlsson received the M.Sc. and Ph.D. degrees from the Lund Institute of Technology, Lund, Sweden, in 1988 and 1995, respectively.

His postgraduate research included radio wave propagation analysis for both micro and pico cell structures for wireless communications systems as well as the design of related measurement equipment. During this period, he was an active Member of the EU project COST 231 and the Swedish delegate of COST 259. In 1995, he joined the Radio System Group at Telia Research AB, Malmö, Sweden, working on the design, analysis and network planning of high capacity broadband radio communications systems. He has been active in the standardization of ETSI/BRAN HiperLAN2 and Chairs the regulatory group of HiperLAN2 Global Forum (H2GF). During 2000, he was a research Fellow at the Department of Electrical & Electronic Engineering, University of Bristol, Bristol, U.K., in combination with a part-time position at Telia Research AB. He then became Manager of the Mobile System Innovation area at Telia Research AB until 2002, when he was appointed Expert in radio communications, a position he is now holding at TeliaSonera AB.